Synchronous Deglacial Overturning and Water Mass Source Changes

Natalie L. Roberts, *et al.*

Science **327**, 75 (2009);
DOI: 10.1126/science.1178068

Synchronous Deglacial Overturning and Water Mass Source Changes

Natalie L. Roberts,[1]* Alexander M. Piotrowski,[1] Jerry F. McManus,[2] Lloyd D. Keigwin[3]

Understanding changes in ocean circulation during the last deglaciation is crucial to unraveling the dynamics of glacial-interglacial and millennial climate shifts. We used neodymium isotope measurements on postdepositional iron-manganese oxide coatings precipitated on planktonic foraminifera to reconstruct changes in the bottom water source of the deep western North Atlantic at the Bermuda Rise. Comparison of our deep water source record with overturning strength proxies shows that both the deep water mass source and the overturning rate shifted rapidly and synchronously during the last deglacial transition. In contrast, any freshwater perturbation caused by Heinrich event 1 could have only affected shallow overturning. These findings show how changes in upper-ocean overturning associated with millennial-scale events differ from those associated with whole-ocean deglacial climate events.

Changes in ocean overturning affect regional climate through the redistribution of heat energy to the high latitudes (*1*). Reconstructions of past ocean circulation changes suggest a strong link between the strength of Atlantic Meridional Overturning Circulation (AMOC) and circum–North Atlantic temperatures, as evidenced by the close match between rapid shifts in nutrient proxy records (*2*) and Greenland ice core paleotemperature records (*3*). Models of thermohaline circulation have suggested rapid changes in overturning strength and water mass stratification during meltwater-forced events, but also suggest that rate of overturning can be decoupled from stratification changes. However, changes in these primary physical variables cannot be unambiguously reconstructed through time by means of nutrient proxies of ocean circulation, because their sensitivity to source, circulation, and biological change complicates interpretation. This study directly compares water mass source changes, reconstructed using Nd isotopes, with $^{231}Pa/^{230}Th_0$ ratios recording overturning rates at the same site.

Nd isotopes can be used as a water mass source proxy because (i) the $^{143}Nd/^{144}Nd$ ratio (ε_{Nd}) is a tracer of deep water masses originating in different ocean basins (*4*, *5*); (ii) the 500- to 1000-year residence time of Nd in the ocean (*6*) is shorter than the time required for whole-ocean mixing; and (iii) Nd isotopes are not fractionated by biological or low-temperature processes (*7*). The ε_{Nd} value for North Atlantic Deep Water (NADW) is ~ –14, and for Antarctic Bottom Water (AABW) it is ~ –7 to –9 (*4*, *5*, *7*), at modern deep water formation sites. Nd isotopes can be used to track these water masses over long path lengths (*7*). In marginal settings with high suspended particle concentrations, the water mass ε_{Nd} appears to be altered by exchange with sedimentary Nd (*8*). Our site on the northeast Bermuda Rise (Fig. 1) is in the open ocean, oceanographically distant from major continental boundaries, and not located downstream of Bermuda. Although sediment deposition rates are high, the particles are primarily transported by recirculating gyres and any leachable material is predominantly authigenic (*9*). Application of ε_{Nd} together with other oceanographic proxies provides accurate reconstructions of ocean circulation and changes in climate.

Recent millennial-scale Nd isotope studies have used Fe-Mn oxides leached from bulk detrital sediment (*10*). However, horizontal advection of fine sediments (*11*) can transport distal Nd

[1]Godwin Laboratory for Palaeoclimate Research, Department of Earth Sciences, University of Cambridge, Cambridge CB2 3EQ, UK. [2]Department of Earth and Environmental Science, Lamont-Doherty Earth Observatory of Columbia University, Palisades, NY 10964, USA. [3]Department of Geology and Geophysics, Woods Hole Oceanographic Institution, Woods Hole, MA 02543, USA.

*To whom correspondence should be addressed. E-mail: nr297@cam.ac.uk

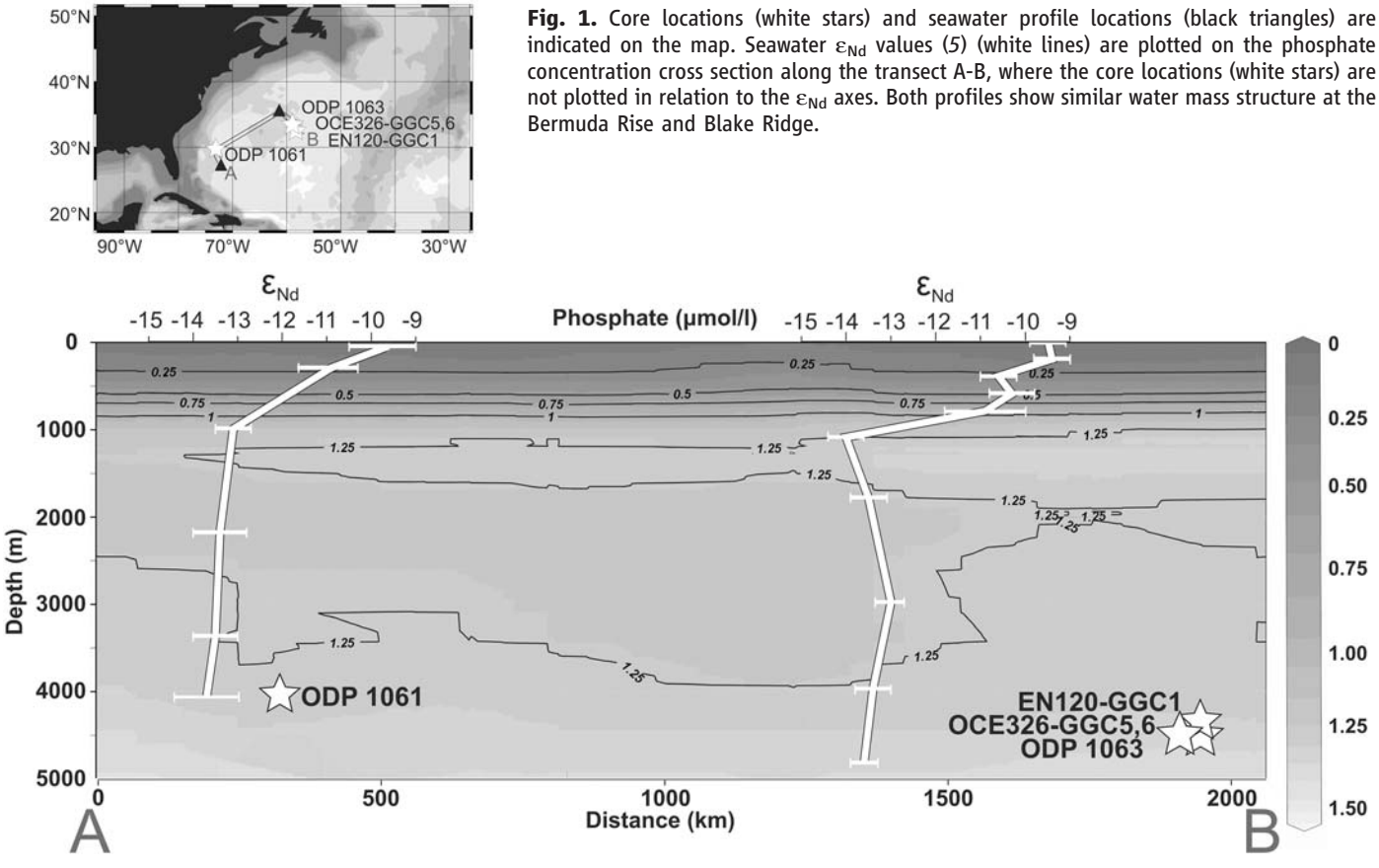

Fig. 1. Core locations (white stars) and seawater profile locations (black triangles) are indicated on the map. Seawater ε_{Nd} values (*5*) (white lines) are plotted on the phosphate concentration cross section along the transect A-B, where the core locations (white stars) are not plotted in relation to the ε_{Nd} axes. Both profiles show similar water mass structure at the Bermuda Rise and Blake Ridge.

isotopic signatures, complicating reconstruction of deep water composition. This is particularly problematic for sediment drift deposits. The Bermuda Rise has deposition rates reaching 100 cm per 1000 years, with >63 μm–sized fraction as low as 0.25%, allowing submillennial resolution, but also indicating sediment transport (*11*, *12*). Alternative phases such as fish teeth (*13*) or benthic foraminiferal calcite (*14*) are typically in low abundance, precluding high-resolution records. In this study we developed an earlier method established by Palmer and Elderfield (*15*) using Fe-Mn oxide coatings on planktonic foraminifera, which are underpinned by fish teeth measurements where possible, from core OCE326-GGC6 (GGC6; 33°41.443′N, 57°34.559′W, 4541 m) (*9*).

Previous studies have shown that Nd is incorporated into foraminiferal calcite at very low concentrations (*16*, *17*); for example, off the coast of Somalia, plankton tow Nd concentrations average 0.11 ppm (*17*), relative to core top measurements in this study of 2.63 ppm. Thus, high Nd concentrations exhibited by planktonic foraminifera from sediment cores likely result from metal oxide coatings on the shell (*17*). The precipitation of Fe-Mn oxide coatings onto sediment particles has been demonstrated to take place at the sediment-water interface (*10*, *15*). Dissolved Nd concentrations increase with depth in the water column (*18*), and because sediment particles are in contact with Nd-rich bottom waters far longer than with other water masses, they retain a bottom water signature. All reductively cleaned and uncleaned foraminifera [calcite plus coating, with all clay and silicates removed (*9*)] at three North Atlantic core tops are within error of each other and the bottom water (NADW) composition (Fig. 2). The reductively cleaned foraminifera fall along mixing curves predicted by plankton tow end members, in the direction of surface water concentrations and ε_{Nd} values. We calculate that in order to obtain surface water values, between 90 and >98% of all coatings must be removed; any remaining coatings are likely due to inefficient cleaning or readsorption of Nd onto clean calcite during cleaning (*17*). Because planktonic foraminifera Fe-Mn oxide coatings accurately archive bottom water ε_{Nd} at the Bermuda Rise, this may be a promising approach in regions of high sediment accumulation (*9*).

Downcore Nd isotope measurements were made on bulk sediment leachate (*10*), reductively cleaned and uncleaned planktonic foraminifera, and reductively cleaned fish debris from Bermuda Rise core GGC6 (Fig. 3). Although core top bulk sediment leachate ε_{Nd} values are within error of modern-day NADW (*4*, *5*) (Fig. 2), downcore measurements are always more positive than the foraminiferal and fish debris ε_{Nd} and do not record the same changes as benthic $\delta^{13}C$ (*Cibicidoides wuellerstorfi*, epibenthic) from nearby Bermuda Rise core EN120-GGC1 (33°40′N; 57°37′W, 4450 m) (*19*). This suggests variable addition of a radiogenic Nd contribution to the bulk sediment leachate record. One plausible source is volcanic ash transported southward by bottom currents (*11*), providing a source of more positive Nd isotopic composition mobilized during leaching. Because foraminifera are not transported horizontally by currents (*11*), the observation that the uncleaned foraminifera and fish debris have no significant deviation from a 1:1 relationship throughout the record (fig. S2) confirms that we are measuring Fe-Mn oxide coatings precipitated on the planktonic foraminifera shells in bottom waters at the Bermuda Rise, as does the finding that core top samples match local deep water. The overall trend of the uncleaned foraminifera Nd isotopes ($\varepsilon_{Nd\text{-}UF}$), from more radiogenic southern source deep water (SSW) values in the glacial to less radiogenic northern source values in the Holocene, is consistent with benthic $\delta^{13}C$ at this site and elsewhere (*20*).

Changes in the strength of AMOC are believed to cause variations in the $^{231}Pa/^{230}Th_0$ ratio (*21*, *22*) because faster overturning rates will result in a higher flux of Pa to the Southern Ocean relative to more particle-reactive Th, lowering the sedimentary $^{231}Pa/^{230}Th_0$ ratio in the North Atlantic (*23*). Measurements of planktonic and benthic $^{12}C/^{14}C$ ($\Delta^{14}C_{B\text{-}P}$) provide another means of estimating AMOC rate, because the age difference between the two samples indicates the time since ventilation. However, these proxies are not without ambiguities. Sedimentary $^{231}Pa/^{230}Th_0$

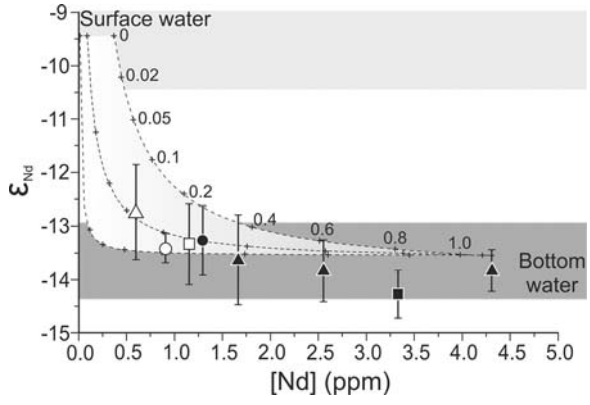

Fig. 2. Core top measurements of reductively cleaned (open symbols) and unclean planktonic foraminifera (solid symbols) from cores ODP172 1061 (circles), OCE326-GGC6 (triangles), and ODP172 1063 (squares). Mixing curves are plotted on the basis of surface and deep water ε_{Nd} measurements (*5*) and average plankton tow Nd concentrations (0.11064 ppm; center dashed line) and minimum and maximum envelopes (0.01224 ppm and 0.34992 ppm, respectively) (*17*), and the maximum measured Fe-Mn coating Nd concentration. Surface water (light gray) and bottom water (dark gray) ε_{Nd} values are indicated by bands including 2σ errors (*5*). Numbers denote the fraction of Fe-Mn oxide coatings contributing to the ε_{Nd} signal.

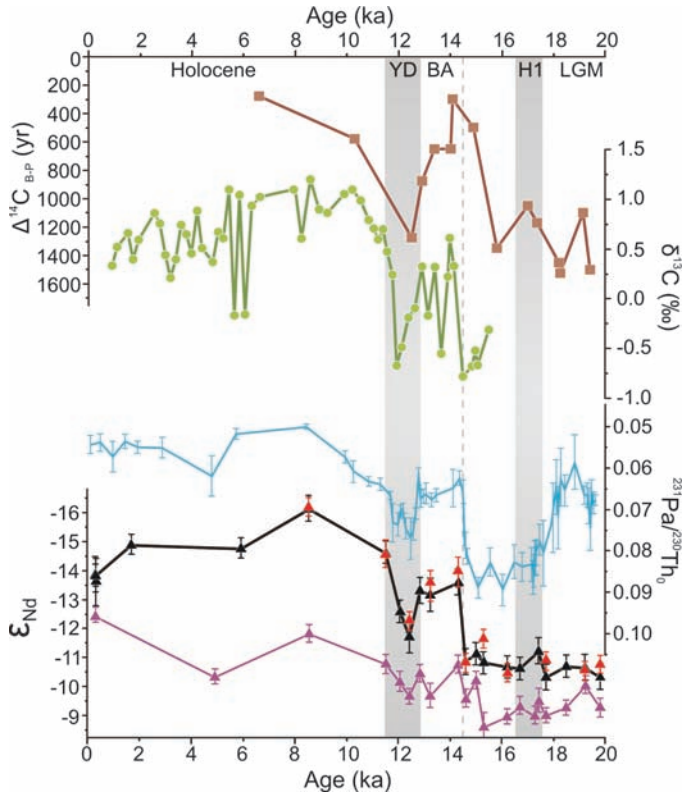

Fig. 3. GGC6 sediment leachates (purple triangles), unclean foraminifera (black triangles), and reductively cleaned fish debris (red triangles), plotted with GGC5 $^{231}Pa/^{230}Th_0$ ratios (blue line) (*22*), GGC1 benthic $\delta^{13}C$ (green circles) [(*19*); for age model see (*9*)], and $\Delta^{14}C$ paired benthic and planktonic apparent ventilation ages (brown squares) (*25*, *26*). The Holocene, Younger Dryas (YD), Bølling-Allerød (BA), Heinrich event 1 (H1), and 14,600 years ago (gray dashed line) are indicated; ka, thousands of years ago. Modern NADW ε_{Nd} ~ –14 and AABW ε_{Nd} ~ –7 to –9 (*4*, *5*, *7*).

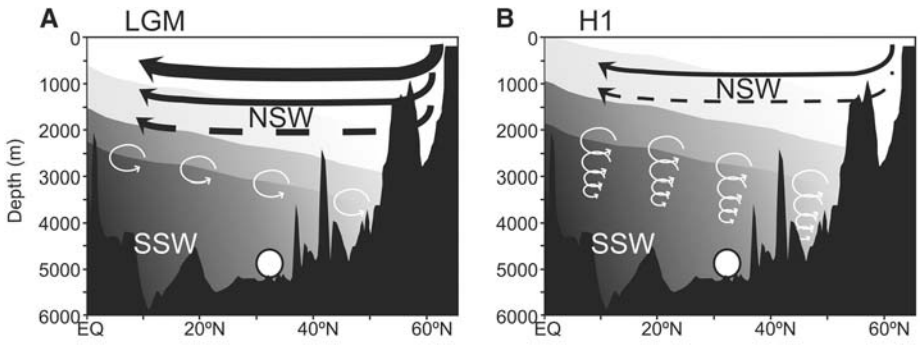

Fig. 4. Schematic illustration of ocean circulation over the Bermuda Rise (white circle) at (**A**) the LGM, and (**B**) Heinrich event 1. ε_{Nd} is represented by grayscale from more negative (light gray) to less negative (dark gray), with the relative overturning strength of NSW (black arrows) and the relative effect of vertical mixing on water mass ε_{Nd} (white arrows).

records may also be influenced by variable scavenging due to variations in particle flux and sediment composition, particularly opal (*24*). Deep water $\Delta^{14}C$ can also be influenced by the mixing of potentially varying and poorly constrained end members. The $\varepsilon_{Nd\text{-}UF}$ and $^{231}Pa/^{230}Th_0$ shifts are sharp, coincident, and correlated across the deglacial climate transitions (the Bølling-Allerød–Younger Dryas–Holocene variations). $\varepsilon_{Nd\text{-}UF}$ trends also match a composite $\Delta^{14}C_{B\text{-}P}$ apparent ventilation record produced from benthic and planktonic foraminifera and bivalves from deep sites throughout the western North Atlantic, confirming that these are basinwide changes (*25*, *26*).

The $\varepsilon_{Nd\text{-}UF}$ record (Fig. 3) allows us to make inferences about how AMOC source changes relate to ventilation and overturning rate. The Last Glacial Maximum (LGM) $\varepsilon_{Nd\text{-}UF}$ data record a bottom water composition of ~ –10.6, indicating the influence of SSW in the deep glacial Atlantic, an interpretation supported by $\delta^{13}C$ data (*2*, *20*) and leachate Nd isotope data from the South Atlantic Cape Basin (*10*). Both Nd isotopes and $\Delta^{14}C_{B\text{-}P}$ remained constant from 20,000 to 14,600 years ago, indicating unchanged water mass source and overturning strength in the deep between the LGM and Heinrich event 1. Conversely, $^{231}Pa/^{230}Th_0$ shifted to higher values by 17,500 years ago, which was interpreted as a strong reduction in AMOC by McManus *et al.* (*22*). The fact that $\varepsilon_{Nd\text{-}UF}$ did not reach SSW end-member values (*27*), combined with a constant gradient of 3.5 ε units between the Bermuda Rise and the Cape Basin (*10*), suggests that some proportion of northern source water (NSW) was continuously advected southward and is evidence against a total shutdown of AMOC. It also suggests that $^{231}Pa/^{230}Th_0$ ratios that approach the production ratio must at least in part be due to opal fluxes increasing the ratio (*28*), but does not fully elucidate the effect of opal flux. However, with evidence of moderate opal fluxes at the LGM (*28*), any correction on $^{231}Pa/^{230}Th_0$ necessitates LGM values that indicate overturning similar to or stronger than the Holocene or Bølling-Allerød. Because the deep $\Delta^{14}C_{B\text{-}P}$ and $\varepsilon_{Nd\text{-}UF}$ records see a relatively small contribution from NSW during the LGM, $^{231}Pa/^{230}Th_0$ is likely integrating the entire water column and primarily recording fast, shallow overturning of glacial intermediate NSW (*22*). This is concordant with increasing evidence from other proxies supporting a fast, shallow overturning cell at the LGM (*20*, *23*, *26*, *29*, *30*).

Our results support the necessity for relatively fast overturning at the LGM in order to maintain a steep vertical chemical gradient in the northwest Atlantic (*20*) under conditions of strong vertical mixing (*31*) (Fig. 4A). If freshwater perturbation induced by Heinrich event 1 slowed overturning, it affected only the upper ocean (*30*), resulting in constant deep $\Delta^{14}C_{B\text{-}P}$ ventilation rates and an increase in the $^{231}Pa/^{230}Th_0$ ratio integrated through the water column. With slower overturning, the strong vertical mixing would have weakened the chemical gradient, allowing more NSW to be transported to depth. This would have offset any effect of decreased NSW production and shoaling of AABW, and would have resulted in no significant change in the Nd isotopic signature at this site (Fig. 4B). Because there were no changes in the boundary conditions at this time, Heinrich event 1 may be likened to modeling results indicating relatively gradual changes in overturning rates during glacial freshwater perturbation (*32*).

In contrast, all three deep water proxies, as well as the integrated $^{231}Pa/^{230}Th_0$ ratio shift during the deglacial events starting at 14,600 years ago, invoke whole-ocean change in both overturning rate and water mass source, similar to jumps in state via hysteresis behavior (*32*). This is evidence for two different ocean circulation responses to climate forcing, which suggests that glacial millennial-scale changes in shallow overturning are inherently different from Milankovitch-forced glacial-interglacial changes, because the latter are accompanied by shifts in boundary conditions and whole water column reorganization.

The large deglacial shifts in benthic $\delta^{13}C$ and the constant ε_{Nd} gradient between the North and South Atlantic from 20,000 to 14,600 years ago suggest no change in the NSW end member. However, the early Holocene ε_{Nd} value of –16 recorded by foraminifera and fish teeth indicates that NSW was 2 ε units more negative than modern NADW. This suggests an increased proportion of the Labrador Sea component of NADW, which is thought to have begun advecting at ~8000 years ago (*33*).

Fe-Mn oxide coatings that are precipitated onto planktonic foraminifera reliably record bottom water ε_{Nd} at the Bermuda Rise today, and provide an accurate archive of past water mass structure changes in areas of sediment redistribution. If meltwater at Heinrich event 1 did affect ocean overturning, it was most likely in the upper part of the water column, enhancing the effects of vertical mixing and resulting in unchanging chemical signatures in the deep. This calls for modeling studies that distinguish between intermediate and deep overturning changes and do not invoke total shutdown of AMOC. After 14,600 years ago we observe coupled North Atlantic water mass source and overturning strength shifts through deglacial climate events linking the relative proportion of NSW and SSW with rates of overturning. There is invariably a strong ocean-climate link over the last deglacial, but the sensitivity of this link must be tested during more stable times (for example, the Holocene) in order to determine future climate change implications.

References and Notes

1. W. S. Broecker, G. H. Denton, *Geochim. Cosmochim. Acta* **53**, 2465 (1989).
2. E. A. Boyle, L. Keigwin, *Nature* **330**, 35 (1987).
3. W. Dansgaard *et al.*, *Nature* **364**, 218 (1993).
4. D. J. Piepgras, G. J. Wasserburg, *Science* **217**, 207 (1982).
5. D. J. Piepgras, G. J. Wasserburg, *Geochim. Cosmochim. Acta* **51**, 1257 (1987).
6. K. Tachikawa, V. Athias, C. Jeandel, *J. Geophys. Res.* **108**, 3254 (2003).
7. S. L. Goldstein, S. Hemming, in *Treatise on Geochemistry*, H. Elderfield, Ed. (Elsevier, Oxford, 2003), vol. 6, pp. 453–489.
8. F. Lacan, C. Jeandel, *Earth Planet. Sci. Lett.* **232**, 245 (2005).
9. See supporting material on *Science* Online.
10. A. M. Piotrowski, S. L. Goldstein, S. R. Hemming, R. G. Fairbanks, *Science* **307**, 1933 (2005).
11. I. N. McCave, *Science* **298**, 1186 (2002).
12. L. D. Keigwin, G. A. Jones, *Deep Sea Res.* **36**, 845 (1989).
13. E. E. Martin, B. A. Haley, *Geochim. Cosmochim. Acta* **64**, 835 (2000).
14. V. Klevenz, D. Vance, D. N. Schmidt, K. Mezger, *Earth Planet. Sci. Lett.* **265**, 571 (2008).
15. M. R. Palmer, H. Elderfield, *Earth Planet. Sci. Lett.* **73**, 299 (1985).
16. M. R. Palmer, *Earth Planet. Sci. Lett.* **73**, 285 (1985).
17. C. Pomiès, G. R. Davies, S. M.-H. Conan, *Earth Planet. Sci. Lett.* **203**, 1031 (2002).
18. H. Elderfield, M. J. Greaves, *Nature* **296**, 214 (1982).
19. L. D. Keigwin, G. A. Jones, S. J. Lehman, *J. Geophys. Res.* **96**, 16811 (1991).
20. W. B. Curry, D. W. Oppo, *Paleoceanography* **20**, PA1017 (2005).
21. J. M. Gherardi *et al.*, *Paleoceanography* **24**, PA2204 (2009).
22. J. F. McManus, R. Francois, J.-M. Gherardi, L. D. Keigwin, S. Brown-Leger, *Nature* **428**, 834 (2004).
23. E.-F. Yu, R. Francois, M. P. Bacon, *Nature* **379**, 689 (1996).
24. Z. Chase, R. F. Anderson, M. Q. Fleisher, P. W. Kubik, *Earth Planet. Sci. Lett.* **204**, 215 (2002).
25. L. D. Keigwin, E. A. Boyle, *Paleoceanography* **23**, PA1101 (2008).

26. L. F. Robinson *et al.*, *Science* **310**, 1469 (2005).
27. L. F. Robinson, T. van de Flierdt, *Geology* **37**, 195 (2009).
28. I. M. Gil, L. D. Keigwin, F. G. Abrantes, *Paleoceanography*, **24**, PA4101 (2009).
29. H. K. Evans, I. R. Hall, *Geochem. Geophys. Geosyst.* **9**, Q03023 (2008).
30. S. K. Praetorius, J. F. McManus, D. W. Oppo, W. B. Curry, *Nat. Geosci.* **1**, 449 (2008).
31. C. Wunsch, *Quat. Sci. Rev.* **22**, 371 (2003).
32. A. Ganopolski, S. Ramstorf, *Nature* **409**, 153 (2001).
33. C. Hillaire-Marcel, A. de Vernal, G. Bilodeau, A. J. Weaver, *Nature* **410**, 1073 (2001).
34. Supported by UK NERC grant NE/D002206/1, RG43765/LBZG021, "Assessing the role of ocean circulation in rapid climate change through the novel integration of high-resolution proxy records," and by NSF and the Comer Science and Education Fund (J.M.). We thank A. Galy, D. Hodell, and L. Skinner for discussion; E. Martin for advice on fish teeth cleaning; and J. Clegg and A. Scrivner for help in the lab.

Supporting Online Material
www.sciencemag.org/cgi/content/full/327/5961/75/DC1
SOM Text
Figs. S1 and S2
Tables S1 to S6
References

22 June 2009; accepted 26 October 2009
10.1126/science.1178068

Human Genome Sequencing Using Unchained Base Reads on Self-Assembling DNA Nanoarrays

Radoje Drmanac,[1]* Andrew B. Sparks,[1]† Matthew J. Callow,[1]† Aaron L. Halpern,[1]† Norman L. Burns,[1]† Bahram G. Kermani,[1]† Paolo Carnevali,[1]† Igor Nazarenko,[1]† Geoffrey B. Nilsen,[1]† George Yeung,[1]† Fredrik Dahl,[1]†‡ Andres Fernandez,[1]† Bryan Staker,[1]† Krishna P. Pant,[1]† Jonathan Baccash,[1] Adam P. Borcherding,[1] Anushka Brownley,[1] Ryan Cedeno,[1] Linsu Chen,[1] Dan Chernikoff,[1] Alex Cheung,[1] Razvan Chirita, [1] Benjamin Curson,[1] Jessica C. Ebert,[1] Coleen R. Hacker,[1] Robert Hartlage,[1] Brian Hauser,[1] Steve Huang,[1] Yuan Jiang,[1] Vitali Karpinchyk,[1] Mark Koenig,[1] Calvin Kong,[1] Tom Landers,[1] Catherine Le,[1] Jia Liu,[1] Celeste E. McBride,[1] Matt Morenzoni,[1] Robert E. Morey,[1]§ Karl Mutch,[1] Helena Perazich,[1] Kimberly Perry,[1] Brock A. Peters,[1] Joe Peterson,[1] Charit L. Pethiyagoda,[1] Kaliprasad Pothuraju,[1] Claudia Richter,[1] Abraham M. Rosenbaum,[2] Shaunak Roy,[1] Jay Shafto,[1] Uladzislau Sharanhovich,[1] Karen W. Shannon,[1]‖ Conrad G. Sheppy,[1] Michel Sun,[1] Joseph V. Thakuria,[2] Anne Tran,[1] Dylan Vu,[1] Alexander Wait Zaranek,[2] Xiaodi Wu,[3] Snezana Drmanac,[1] Arnold R. Oliphant,[1] William C. Banyai,[1] Bruce Martin,[1] Dennis G. Ballinger,[1]* George M. Church,[2] Clifford A. Reid[1]

Genome sequencing of large numbers of individuals promises to advance the understanding, treatment, and prevention of human diseases, among other applications. We describe a genome sequencing platform that achieves efficient imaging and low reagent consumption with combinatorial probe anchor ligation chemistry to independently assay each base from patterned nanoarrays of self-assembling DNA nanoballs. We sequenced three human genomes with this platform, generating an average of 45- to 87-fold coverage per genome and identifying 3.2 to 4.5 million sequence variants per genome. Validation of one genome data set demonstrates a sequence accuracy of about 1 false variant per 100 kilobases. The high accuracy, affordable cost of $4400 for sequencing consumables, and scalability of this platform enable complete human genome sequencing for the detection of rare variants in large-scale genetic studies.

Genotyping technologies have enabled the routine assessment of common genetic variants at up to a million sites across the genome in thousands of individuals (*1*) and have increased our understanding of human genetic diversity and its biological and medical impact. Whole-genome sequencing costs have dropped from the >$100 million cost of the first human genomes (*2*, *3*) to the point where individual labs have generated genome sequences in a matter of months for material costs of as low as $48,000 (*4*–*12*) (table S5). Sequencing technologies, which use a variety of genomic microarray construction methodologies and sequencing chemistries (*13*–*32*), can determine human genetic diversity over an entire genome and identify common as well as rare single-nucleotide polymorphisms (SNPs), insertions, and deletions. Despite these advances, improvements are still needed to enable the cost-effective characterization of the many hundreds of genomes required for genetic studies of complex diseases and for personalized disease prevention, prognosis, and treatment.

We generated sequencing substrates [Fig. 1A and supporting online material (SOM)] by means of genomic DNA (gDNA) fragmentation and recursive cutting with type IIS restriction enzymes and directional adapter insertion (Fig. 1B and fig. S1). The resulting circles were then replicated with *Phi*29 polymerase (RCR) (*33*). Using a controlled, synchronized synthesis, we obtained hundreds of tandem copies of the sequencing substrate in palindrome-promoted coils of single-stranded DNA, referred to as DNA nanoballs (DNBs) (Fig. 1C). DNBs were adsorbed onto photolithographically etched, surface-modified (SOM) 25- by 75-mm silicon substrates with grid-patterned arrays of ~300-nm spots for DNB binding (Fig. 1C). The use of patterned arrays increased DNA content per array and image information density relative to random genomic DNA arrays (*6*, *9*, *11*, *14*, *28*). High-accuracy combinatorial probe anchor ligation (cPAL) sequencing chemistry was then used to independently read up to 10 bases adjacent to each of eight anchor sites (Fig. 1D), resulting in a total of 31- to 35-base mate-paired reads (62 to 70 bases per DNB). cPAL is based on unchained hybridization and ligation technology (*15*, *27*, *28*, *31*), previously used to read 6 to 7 bases from each of four adapter sites (26 total bases) (*28*), here extended using degenerate anchors to read up to 10 bases adjacent to each of the eight inserted adapter sites (Fig. 1D, right) with similar accuracy at all read positions (fig. S3). This increased read length is essential for human genome sequencing.

Cell lines derived from two individuals previously characterized by the HapMap Project (*34*), a Caucasian male of European descent (NA07022) and a Yoruban female (NA19240), were sequenced. NA19240 was selected to allow for a comparison of our sequence to the sequence of the same genome currently being assembled by the 1000 Genome Project. In addition, lymphoblast DNA from a Personal Genome Project Caucasian male sample, PGP1 (NA20431) was sequenced because substantial data are available for biological comparisons (*35*–*37*). Automated cluster analysis of the four-dimensional intensity data produced raw base reads and associated raw base scores (SOM).

We mapped these sequence reads to the human genome reference assembly with a custom alignment algorithm that accommodates our read structure (fig. S4), resulting in between 124 and 241 Gb mapped and an overall genome coverage of 45- to 87-fold per genome.

To assess representational biases during circle construction, we assayed genomic DNA and intermediate steps in the library construction process by quantitative polymerase chain reaction

[1]Complete Genomics, Inc., 2071 Stierlin Court, Mountain View, CA 94043, USA. [2]Department of Genetics, Harvard Medical School, Cambridge, MA 02115, USA. [3]School of Medicine, Washington University, St. Louis, St. Louis, MO 63110, USA.

*To whom correspondence should be addressed. E-mail: rdrmanac@completegenomics.com (R.D.); dballinger@completegenomics.com (D.G.B.)

†These authors contributed equally to this work.

‡Present address: Ion Torrent Systems, San Francisco, CA 94158, USA.

§Present address: San Diego State University, San Diego, CA 92115, USA.

‖Present address: Life Technologies, Carlsbad, CA 92008, USA.